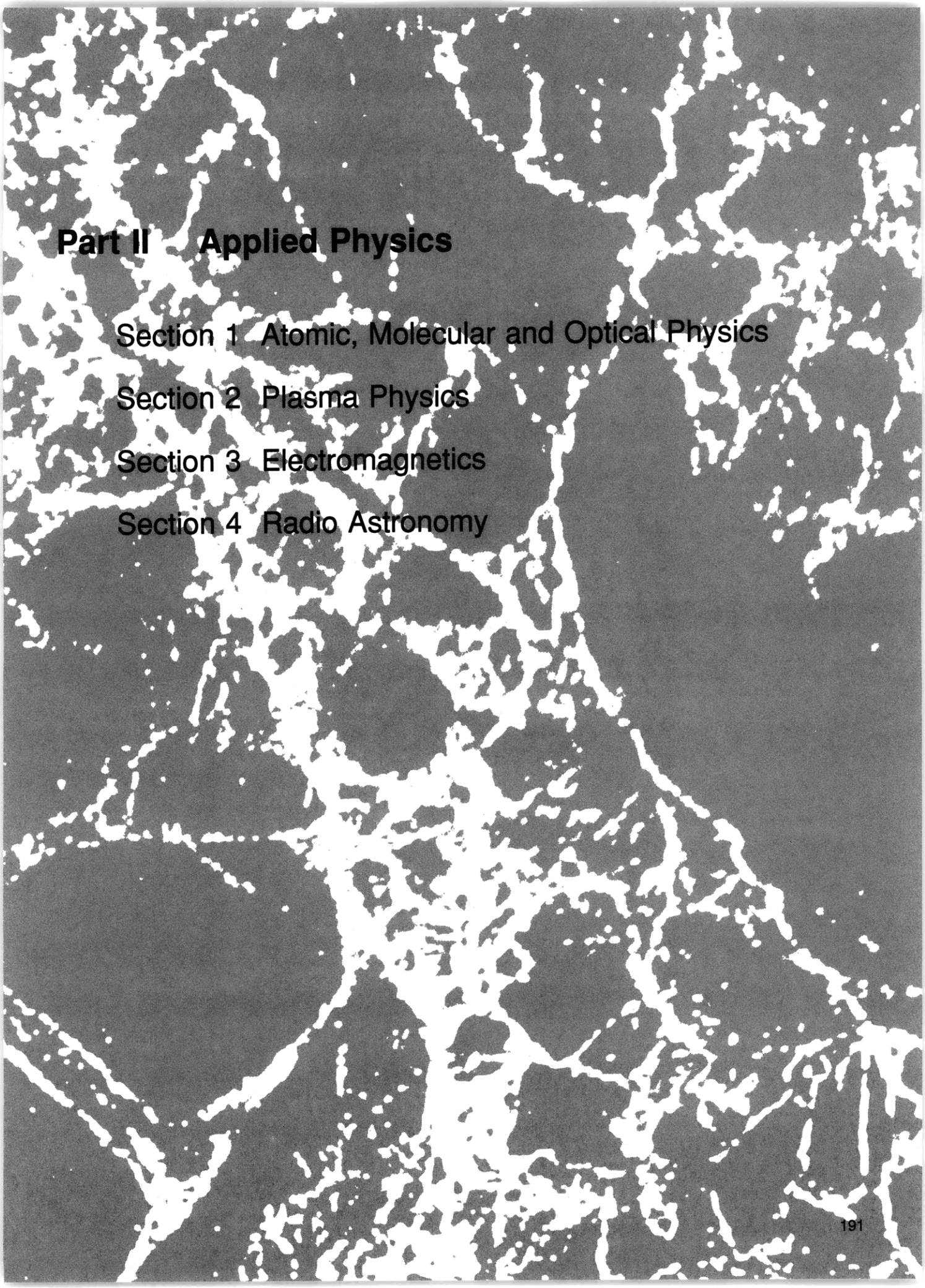

# Part II Applied Physics

# Section 1 Atomic, Molecular and Optical Physics

# Chapter 1. Quantum Optics and Photonics

**Academic and Research Staff**

Professor Shaoul Ezekiel, Dr. Selim M. Shahriar

**Visiting Scientists and Research Affiliates**

Dr. Philip R. Hemmer,[1] Dr. Mara G. Prentiss,[2] John D. Kierstead[1]

**Graduate Students**

John J. Donoghue,[3] Daniel Katz,[2] Juliet Mervis,[2] Stephen P. Smith

**Undergraduate Students**

Arthur Chu[2]

## 1.1 Data Storage Using Raman Induced Optical Spectral Holeburning

**Sponsor**

U.S. Air Force - Electronic Systems Division
Contract F19628-92-K-0013

Optical spectral holeburning in cryogenic materials has generated much recent interest because of its potential for high density optical storage, both in the time and frequency domain and in high speed optical processing.[4] In holeburning materials, storage capacity is determined by the ratio of optical inhomogeneous to homogeneous linewidths (typically $10^6$) at a single position. Optical data rates can be as large as the optical inhomogeneous linewidth (usually in excess of several GHz). In addition, spatial resolution is determined by the optical wavelength, so that the total storage density can be very large, and entire holographic images can be processed at high speed. Although this is impressive, there is still room for substantial improvement.

We have developed a novel technique for enhancing the storage capacity of optical spectral holeburning materials, using Raman coherent population trapping. This technique is based on two properties of the Raman transparent state, namely, the equivalence of the Raman transparent state to a ground-state (spin) coherence[5] and the sensitivity of this transparent state to the difference phase of the optical fields. The first property permits the optical excitation and detection of ground-state (spin) echoes, and the second property allows time-separated optical fields to interfere even after the optical coherence has decayed. Together, these two properties can be used to increase the storage capacity of optical spectral holeburning beyond the current fundamental limit given by the ratio of optical inhomogeneous to homogeneous linewidths.

Raman population trapping, illustrated in figure 1, allows both constructive and destructive interference to occur between time-separated optical fields, even though the optical coherence has long decayed. In the presence of ground-state inhomogeneous broadening, this permits time-domain optical storage. We have demonstrated this effect experimentally using a sodium atomic beam.[6] Figure 2 shows storage and recall of data using Raman induced spin coherence for a variety of conditions.

---

1 Rome Laboratory, Hanscom, Massachusetts.

2 Harvard University, Cambridge, Massachusetts.

3 Tufts University, Medford, Massachusetts.

4 Y.S. Bai and R. Kachru, *Opt. Lett.* 18: 1189 (1993); M. Mitsunaga, R. Yano, and N. Uesugi, *Opt. Lett.* 16: 1890 (1991); B. Kohler, S. Bernet, A. Renn, and U.P. Wild, *Opt. Lett.* 18: 2144 (1994).

5 M.S. Shahriar and P.R. Hemmer, *Phys. Rev. Lett.* 65: 1865 (1990).

6 P.R. Hemmer, M.S. Shahriar, Z. Cheng, J. Kierstead, and M.K. Kim, *Opt. Lett.* 65: 1865 (1994).

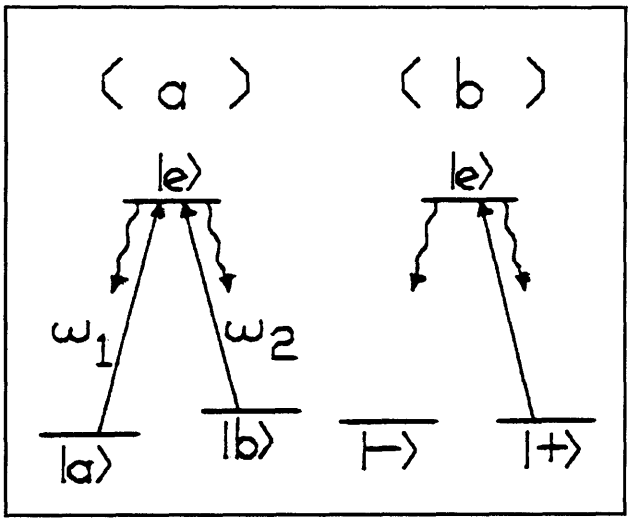


**Figure 1.** (a) Schematic of the resonance Raman interaction. (b) The Raman interaction in the superposition state basis. The |–> state is transparent to the resonant optical fields.

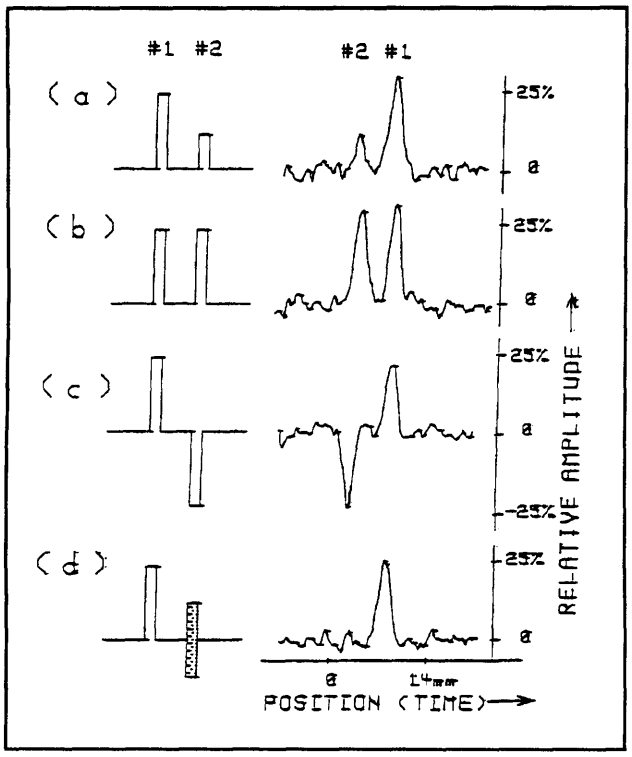


**Figure 2.** Observation of data storage and retrieval using Raman induced spin echo: (a) unequal bits, (b) equal bits, (c) out of phase bits, and (d) $\pi/2$ phase shifted bits.

To show the potential for increased storage density, note that the Raman-excited rf echo storage of figure 2 requires only low-intensity Raman-resonant optical pulses. Thus, for an inhomogeneously broadened optical transition, only atoms corresponding to a single optical spectral hole need participate. This means that many bits of optical data can be stored in a single optical spectral hole. The maximum number of bits per optical spectral hole is ultimately limited by the ratio of the inhomogeneous to homogeneous linewidths of the rf transition. Since the storage capacity of optical spectral holeburning is calculated based on only one data bit per homogeneous width spectral hole, it is clear that the ratio of optical inhomogeneous to homogeneous linewidths no longer defines the storage limit.

Raman population trapping can also be used to increase the storage capacity of time-domain optical holeburning. To see this, recall from figure 1 that the |+> ↔ |e> transition is optically excited and can therefore be used to perform time-domain spectral holeburning, just as any inhomogeneously broadened optical transition. In particular, consider the case of long-term data storage, employing Raman-resonant optical write and read pulses. In this case, long-term information storage is accomplished with a modulated population difference between the |–> and |+> states. But this population difference is also an rf coherence, which dephases in the presence of ground-state inhomogeneous broadening. As a result, the Raman resonant read pulse cannot produce optical echoes unless the ground-state coherence is first rephased, for example by an rf $\pi$-pulse. This suggests that it may be possible to selectively store and recall more than one data set by using time-domain ground-state spectral holeburning to store and retrieve various |–> and |+> state population modulations. These population modulations in turn correspond to the Fourier transforms of individual sets of optical data pulses.

Verification of multiple data set storage and recall, using both Raman and optical time-domain spectral holeburning is accomplished with the pulse sequence of figure 3. As shown, the input consists of two time-separated data/write pulse sets, where each set consists of a pair of Raman resonant optical data pulses followed by a Raman resonant write pulse. Rephasing is accomplished with an rf $\pi$-pulse, and optical echoes are produced by two Raman resonant read pulses applied at appropriate times after the $\pi$-pulse, as illustrated. Note that the rf field excites all the atoms in the material. If spatially localized re-phasing is needed, the rf field can be replaced by intense off-resonance Raman excitation.

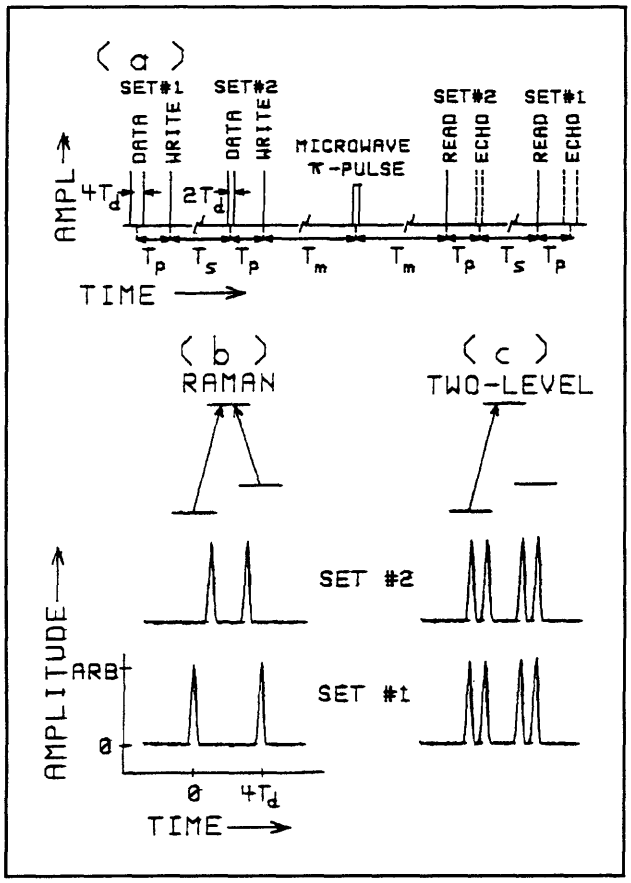


**Figure 3.** Theoretical demonstration of selective storage and recall of two time-separated optical data sets. (a) Pulse sequence used for calculation. (b) Calculated echoes for two-frequency Raman resonant optical pulses, showing selective recall. (c) Echoes for single frequency optical pulses (conventional stimulated optical echoes), showing crosstalk.

The calculated echo signals produced by each of the two Raman resonant read pulses is shown in figure 3b. As seen, Raman-excited time-domain spectral holeburning achieves selective recall of both data sets even though they are separated by much longer than the optical homogeneous decay time. Since the theoretical storage limit of optical spectral holeburning assumes that all data must be input before the optical coherence decays, figure 3b shows the potential for higher storage capacity in the time-domain. In addition, extension of the write window for phase-sensitive data storage has also been shown. For comparison, figure 3c shows calculated echoes for the case of conventional stimulated optical echo storage, modeled by a three-level system, with only one ground-state coupled to the excited-state, as illustrated. In this case, the ground-state populations cannot dephase so that the population modulations created by the two optical data sets are simply summed. Recall of this data at any time simultaneously recalls the data contained in both optical data sets, leading to the crosstalk evident in the echo signals. In the general case of unequal Rabi frequencies, the excitation pulse sequence of figure 3a will produce echo signals which look like a mixture of the two limiting cases of figure 3b and figure 3c (i.e., crosstalk will appear, roughly in proportion to the Rabi frequency difference).

In summary, we have shown how Raman coherent population trapping can be used to increase the optical storage capacity of optical spectral holeburning materials beyond the limit imposed by the ratio of optical inhomogeneous to homogeneous linewidths. This increased storage is based on the ability of Raman coherent population trapping to allow interference even after decay of the optical coherence.

## 1.2 Observation of Cooling Assisted Velocity Selective Coherent Population Trapping

### Sponsor

U.S. Air Force - Electronic Systems Division
Contract F19628-92-K-0013

In recent years, there has been a great deal of interest in velocity selective coherent population trapping (VSCPT).[7] However, since VSCPT occurs via a random walk in momentum space, in order to achieve significant VSCPT in three dimensions, it is necessary to precool and confine atoms close to the recoil limit. We recently predicted[8] that this type of cooling and velocity confinement assisted VSCPT can be achieved in one, two or three dimensions when a $\Lambda$ system atom is excited by a

[7] A. Aspect, E. Arimondo, R. Kaiser, N. Vansteenkiste, and C. Cohen-Tannoudji, *Phys. Rev. Lett.* 61: 826 (1988).

[8] P.R. Hemmer, M.S. Shahriar, M.G. Prentiss, D.P. Katz, K. Berggren, J. Mervis, and N. Bigelow, *Phys. Rev. Lett.* 68: 3148 (1992); M.S. Shahriar, P.R. Hemmer, M.G. Prentiss, P. Marte, J. Mervis, D.P. Katz, N.P. Bigelow, and T. Cai, *Phys. Rev.* A 48: R4034 (1993); M.S. Shahriar, P.R. Hemmer, M.G. Prentiss, A. Chu, D.P. Katz, and N.P. Bigelow, "Phase-Dependent Velocity Selective Coherent Population Trapping in a Folded Three-Level System under Standing Wave Excitation," *Opt. Commun.* 103: 453 (1993); P. Marte, R. Taieb, R. Dum, P. Zoller, M.S. Shahriar, and M.G. Prentiss, *Phys. Rev. A*, forthcoming.

pair of blue detuned Raman resonant standing waves, with a phase difference of $\theta = \pi/4$.

We have recently observed this effect in one dimension using a beam of metastable He atoms.[9]

Figure 4 illustrates schematically the experimental setup, where a diode laser array pumped LNA laser is used to excite the $2^3S_1 - 2^3P_1$ transition at 1.083 micron.

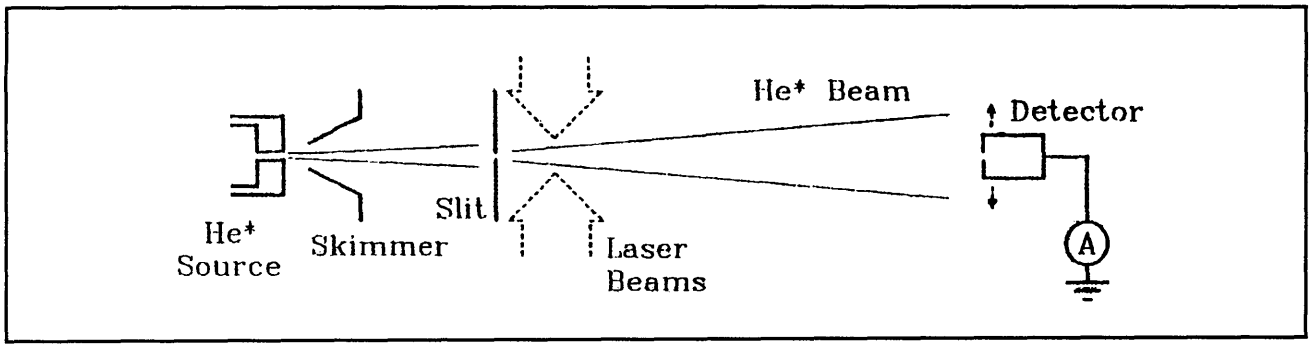


**Figure 4.** Schematic diagram of experimental setup.

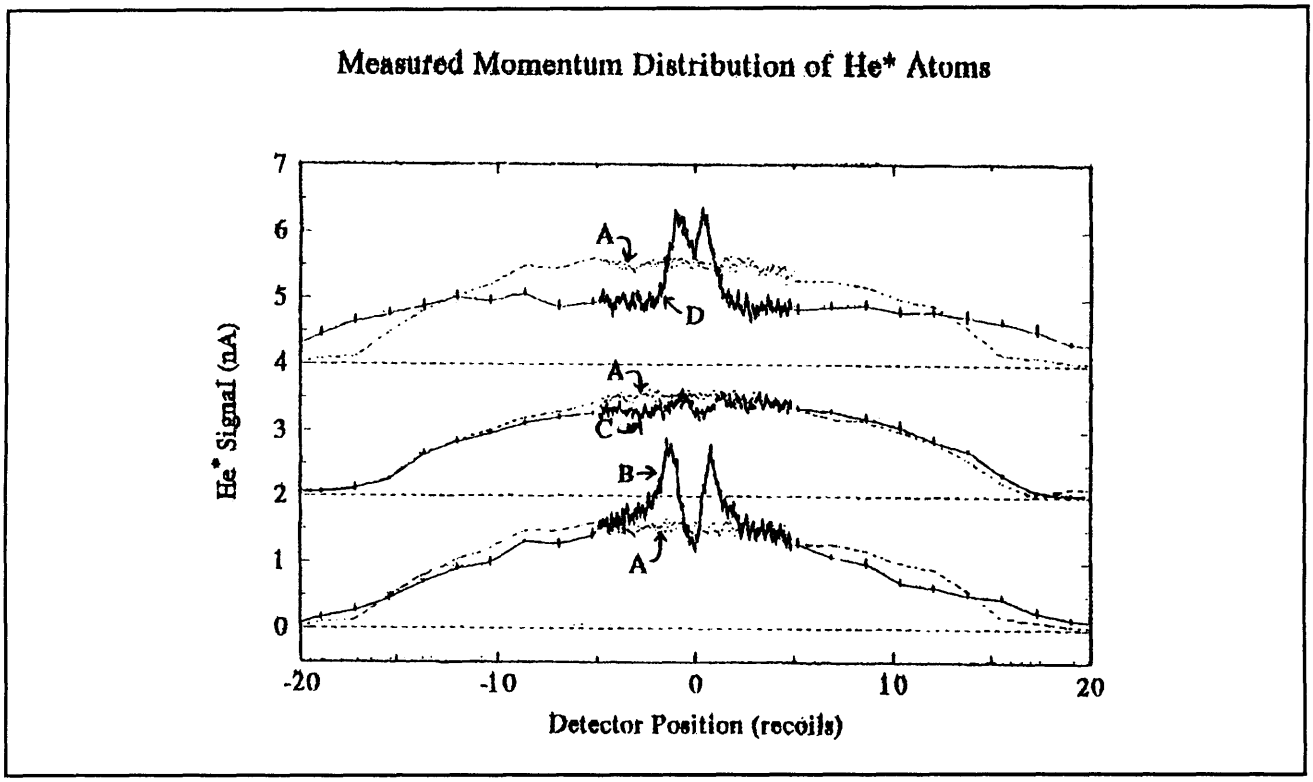


**Figure 5.** Measured momentum distributions of laser cooled He atoms for (A): uncooled atoms, (B): s = 2, $\delta = 0$, (C): s = 0.4, $\delta = 0$, and (D): s = 0.4, $\delta = \Gamma$.

In figure 5, the curves labeled A show the beam profile when the laser is off. With laser on resonance and $\theta = \pi/4$, we studied first the efficiency of VSCPT as a function of the saturation parameter, given by $s = r/(1 + 4\delta^2)$, where r is the laser intensity in units of the saturation intensity, and $\delta$ is the detuning in units of natural linewidth. For s = 2.0, the result is shown by curve B, where VSCPT is

[9] M.S. Shahriar, M.T. Widmer, M.J. Bellanca, E. Vredenbregt, and H.J. Metcalf, "Observation of Cooling Assisted Velocity Selective Coherent Population Trapping," 1994 IC Conference, forthcoming.

manifested by the appearance of the two peaks at $\pm \hbar k$. When s is reduced, the degree of VSCPT is decreased, as expected, since the pumping rate into the dark state is proportional to the mean excited state population, which in turn is proportional to s. Curve C shows the result for $s \cong 0.4$, where the VSCPT peaks are barely visible. We then blue detune the laser by one linewidth ($\delta = 1$) and adjust the intensity to get the same degree of saturation ($s \cong 0.4$). The resulting distribution is shown in curve D. As can be seen, there is strong precooling, with a width of $\pm 2\hbar k$, in agreement with our previous prediction. In addition, the precooling enhances the degree of VSCPT compared to that in curve C, even though the saturation is the same.

Due to the constraints of the present setup, our interaction time is limited to only about 6 recoil times. While this is long enough to observe the precooling, it is too short to see the full extent of the enhancement of VSCPT due to the precooling. Nonetheless, our observation validates the mechanism we had predicted previously, rendering credence to its claim that this scheme would enhance the rate of VSCPT in three dimensions by a factor of 200. This mechanism would allow us to reach a temperature a factor of ten below the recoil limit in about 90 msec.

## 1.3 Suppression of Absorption of Resonance Fluorescence in a Folded Three-Level Atom

### Sponsor

U.S. Air Force - Electronic Systems Division
Contract F19628-92-K-0013

In recent years, there has been a lot of interest in using the $\Lambda$ system atom to reach a very cold temperature via velocity selective coherent population trapping (VSCPT).[10] However, since VSCPT takes a long time, the system is bright initially. To determine what kind of density can be achieved in such a system, it is therefore necessary to look at the density limiting effects during the initial stage when significant VSCPT has not yet taken place. The most important effect is due to the heating caused by absorption of the emission of neighboring atoms.[11]

We have recently found that this absorption is strongly suppressed in the $\Lambda$ system under a very general set of conditions. Tabosa et al. considered various schemes that also experience such suppressions.[12] However, the system we are considering is of great practical interest since a trap employing $\Lambda$ system atoms may be cooled to a temperature substantially below the recoil limit. In addition, this result bodes well for the density achievable in a rectified force trap of $\Lambda$ atoms.[13]

Figure 6a shows how a true $\Lambda$ system can be realized, and figure 6b illustrates the parameters of a $\Lambda$ system. We consider, as an example, the case where the common detuning $\delta$ is blue, as necessary for the scheme of cooling assisted VSCPT.[14] The difference detuning, $\Delta$ is non-zero, as would be the case for the atoms that have not yet undergone VSCPT, and are moving relatively fast. Without affecting the basic feature of the result, we have, for clarity, also assumed that the ground state splitting matches $\Delta$. Figure 7a shows the resonance fluorescence spectrum (RFS) of the $\Lambda$ atom, including the delta function peak at the driving frequency. Figure 7b shows the corresponding gain spectrum. As can be seen, in contrast with a two-level atom, the strongest absorption peaks are far removed from the significant part of RFS. Figure 8 shows the gain spectrum in greater detail. Note that (figure 8c) there is no absorption at the central peak of RFS, and one of the big sidebands of RFS sees loss while the other sees gain. The net result is that the heating due to rescattering force in such a system would be far smaller than that in a two-level system.

---

10 A. Aspect, E. Arimondo, R. Kaiser, N. Vansteenkiste, and C. Cohen-Tannoudji, *Phys. Rev. Lett.* 61: 826 (1988).

11 D.W. Sesko, T.G. Walker, and C. Wieman, *J. Opt. Soc. Am. B* 8: 946 (1991).

12 J.W.R. Tabosa, G. Chen, Z. Hu, R.B. Lee, and H. Kimble, *Phys. Rev. Lett.* 66: 3245 (1991).

13 M.S. Shahriar, P.R. Hemmer, M.G. Prentiss, A. Chu, D.P. Katz, and N.P. Bigelow, Phase-Dependent Velocity Selective Coherent Population Trapping in a Folded Three-Level System under Standing Wave Excitation, *Opt. Commun.* 103: 453 (1993).

14 M.S. Shahriar, P.R. Hemmer, M.G. Prentiss, P. Marte, J. Mervis, D.P. Katz, N.P. Bigelow, and T. Cai, *Phys. Rev.* A 48: R4034 (1993).

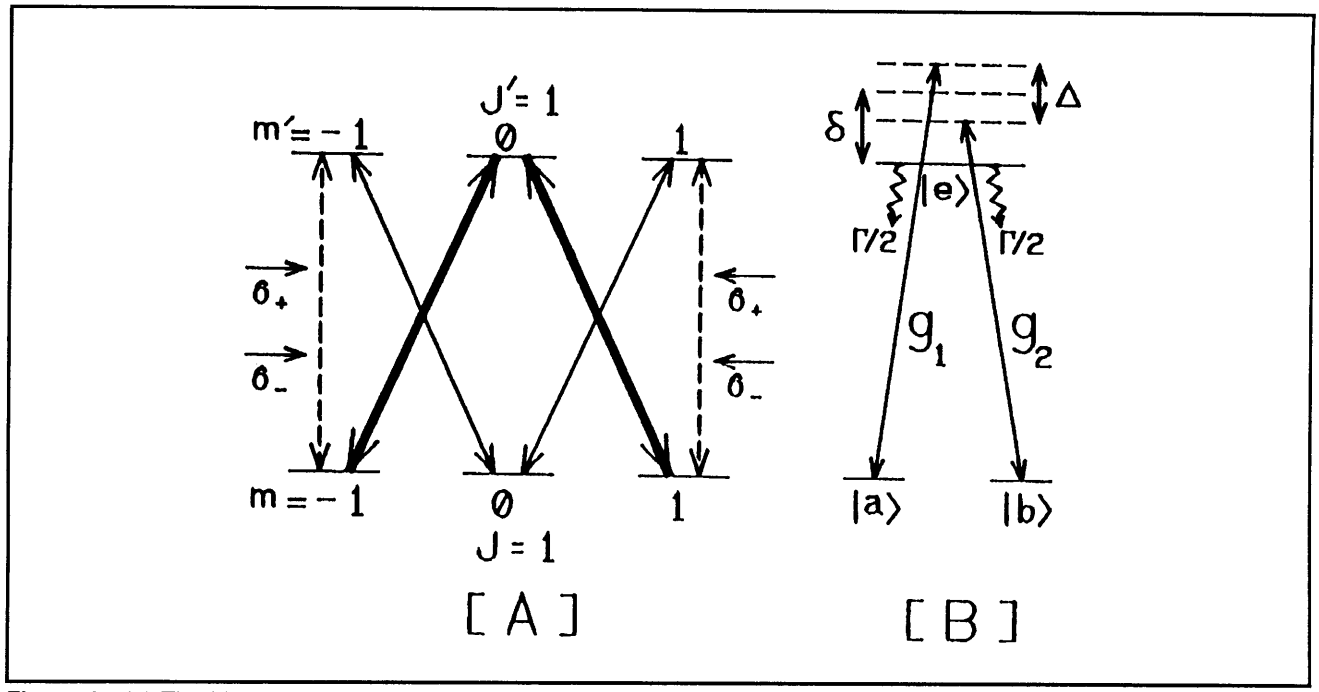


**Figure 6.** (a) The ideal Λ system. (b) Parameters of the Λ system.

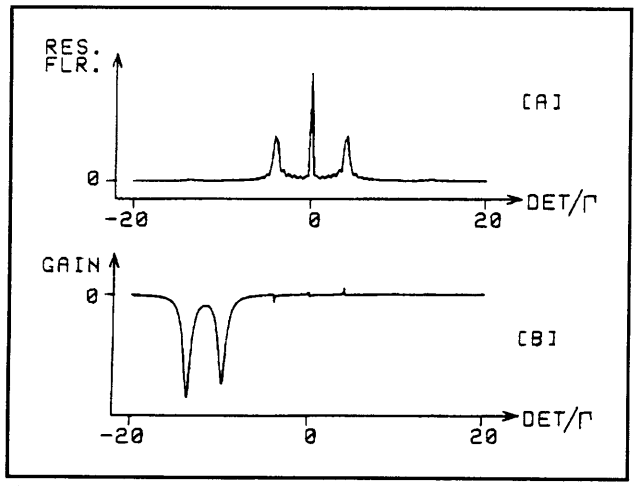


**Figure 7.** (a) Resonance fluorescence spectrum for $g_1 = g_2 = 5.0, \delta = 10.0, \Delta = \pm 4.0$, all in units of Γ. (b) The gain spectrum corresponding to Figure 7a, in arbitrary units.

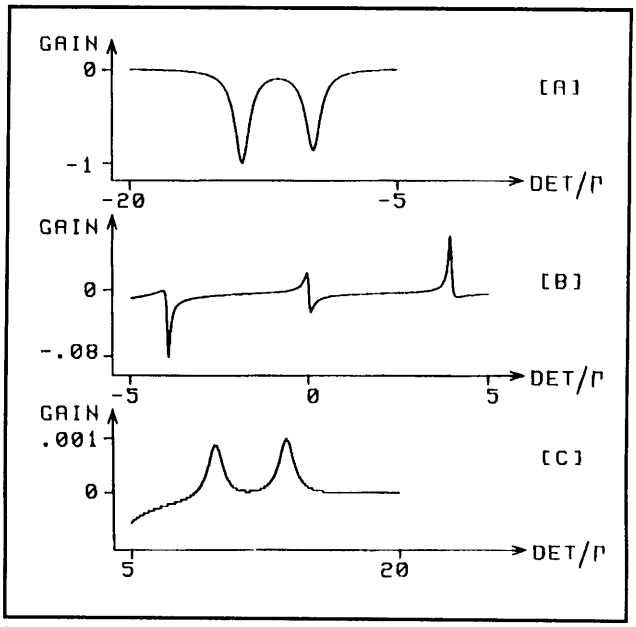


**Figure 8.** Expanded view of the gain spectrum: (a) the two absorption peaks (b) the three central peaks corresponding to the three biggest peaks in the fluorescence spectrum, (c) two very small gain peaks. Note the different vertical scales, normalized to the height of the large absorption peaks in (a).

We find that these results are independent of the sign of Δ, and the relative values of the various parameters.[15] Thus, this suppression of heating applies to the non-zero (positive and negative) velocity atoms in the initial stage of cooling assisted VSCPT. Note also that for the atoms that have undergone VSCPT, the gain spectrum would be similar to figure 7b, while the RFS spectrum vanishes. Thus, these zero velocity atoms see very small heating from the scattering of the hotter atoms. Finally, this scheme may be easily generalized to three dimensions using a J = 1↔J' = 1 transition.

## 1.4 Inversionless Raman Lasing

### Sponsor

U.S. Air Force - Electronic Systems Division
Contract F19628-92-K-0013

There has been much recent interest in the concept of inversionless lasing, primarily for application to high frequency lasers where it is difficult to achieve population inversion.[16] Conventional Raman lasers, while inversionless in the sense that no excited state population is required to produce gain, are not very useful for up-conversion because they still require a population inversion between initial and final states.

Recently, we have studied an inversionless raman laser (IRL) which can not only be used for up-conversion, but has promising potential application to optical phase conjugation and laser frequency translation. The simplest form of IRL is illustrated in figure 9. Here, the Raman laser is pumped by the field at $\omega_c$ and gain is experienced for properly chosen probes at $\omega'_a$ and $\omega'_b$, where the low-frequency pumps at $\omega_a$ and $\omega_b$ empty the final state via coherent population trapping (CPT). This is analogous to gain without inversion (or gain with "hidden" inversion) in the double Λ system, and in fact the calculated "optimum" gain coefficients are of the same order of magnitude. The difference is that it is possible to achieve the optimum gain coefficient over a much wider range of atomic systems. For example, there are no constraints on the relative populations of states |e> and |f> in order to produce gain.

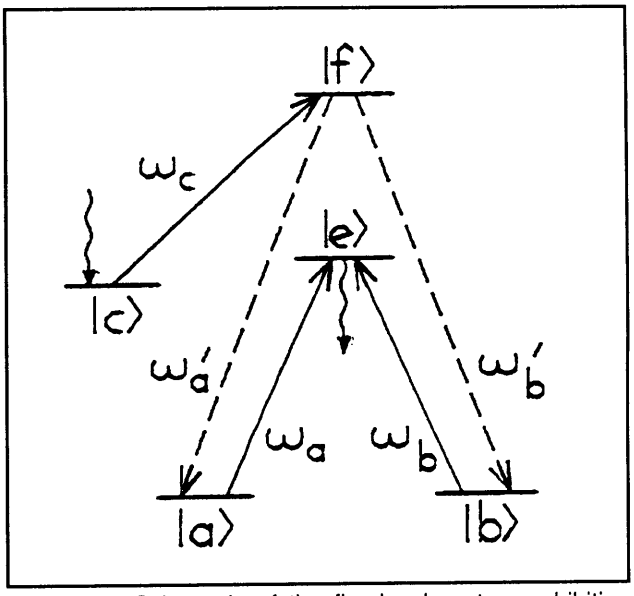


**Figure 9.** Schematic of the five-level system exhibiting inversionless Raman lasing.

Aside from up-conversion, IRL can be used for precise laser frequency translation.[17] This is illustrated in figure 10a. Here, Raman lasing occurs at $\omega'_a$, where $\omega'_b$ acts as the pump and $\omega_a$ is a single, low-frequency optical pumping laser which creates the necessary initial to final state population inversion. Unlike the conventional Raman laser, the IRL scheme of figure 10a allows cw lasing to occur, even if states |a> and |b> are long-lived. For application to optical phase conjugation, the more general four-level IRL scheme of figure 10b is required.[18] This is equivalent to the scheme in figure 4a except that there are two low-frequency pumps so that the necessary inversion is created by CPT, rather than simple optical pumping. This apparently minor distinction leads to significantly larger probe gain coefficients, especially for weak probes. To see why this is the case, recall that in a Raman laser, the gain can be explained in terms of the pump laser scattering off of the ground-state coherence. However, this ground-state coherence must first be generated by the pump and probe beams via CPT, and hence in the weak probe limit,

---

[15] M.S. Shahriar, P.R. Hemmer, and M.G. Prentiss, "Suppression of Absorption of Resonance Fluorescence in a Folded Three-Level Atom," 1994 IC Conference, forthcoming.

[16] M.O. Scully, *Phys. Rep.* 219: 191 (1992); O. Kocharovskaya, *Phys. Rep.* 219: 175 (1992).

[17] M. Poelker and P. Kumar, *Opt. Lett.* 17: 399 (1992).

[18] J. Donoghue, M. Cronin-Golomb, J.S. Kane, and P.R. Hemmer, *Opt. Lett.* 16: 1313 (1991).

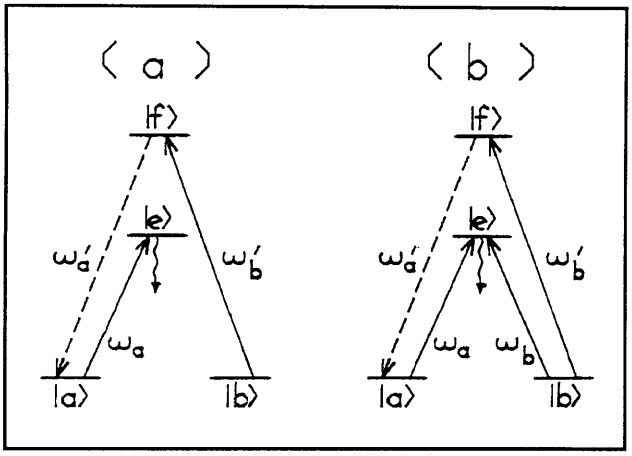


**Figure 10.** Schematic of the four-level double Λ system exhibiting inversionless Raman lasing. (a) Limiting case of single low-frequency pump laser. (b) More general case of two low-frequency pump lasers.

is very small. In contrast, for the IRL scheme of figure 4b the ground state coherence is generated in advance by the low-frequency pump fields. Thus, the pump at $\omega'_b$ can scatter off a ground state coherence, even when no probe is present. Mathematically, this means that the probe gain coefficient diverges as the probe strength approaches zero.

Finally, the ability of IRL to perform optical phase conjugation is a consequence of the differential optical phase sensitivity of Raman gain in the double Λ system. For example, by choosing $\omega_a$ and $\omega'_b$ to be counterpropagating plane waves, and $\omega_b$ to be the input signal beam, IRL generates gain at $\omega'_a$ only for a beam propagating in the conjugate direction.

## 1.5 Creating a Large Angle Coherent Atomic Beamsplitter without a Magnetic Field

### Sponsor

U.S. Air Force - Electronic Systems Division
Contract F19628-92-K-0013

Many atom interferometer applications would benefit from large angle atomic beam splitters with narrow distributions. The interaction between a magnetic field and two standing wave laser fields can provide such a beam splitter.[19] Unfortunately, the required magnetic fields are undesirable in many interferometer applications, and few atomic systems have a suitable transition.

We show that a similar beamsplitter for a three-level atomic system can be obtained in the absence of a magnetic field as long as the excitation fields interacting with the two transitions are standing waves with a differential detuning.[20] This effect can be explained in terms of atomic scattering from dressed state potentials which form a blazed grating, or as the result of a synchronized cycles between Rabi flopping and the precession between between excited states induced by the field detuning. This technique could be used on transitions other than $J = 1 \leftrightarrow J' = 1$.

Consider a three-state system in the basis |a>, |b>, |e>, where the fields interact with the transitions $|a \rightarrow |e$ and $|b \rightarrow |e$. For equal Rabi frequencies and a phase difference of $\pi/2$, the eigenenergies of the Hamiltonian as functions of the atomic position z are shown in figure 11. For states which approach the ground states when the Rabi frequencies tend to vanish, the potentials are given by $\pm (\Delta/2 + |\sin(kz)|)$, where $\Delta$ is the difference detuning, and k is the wave number. In contrast, the state which approaches |e> has a nearly triangular potential.

Figure 12 shows the theoretical momentum distribution for scattering of a monoenergetic atomic beam where all atoms are in |e> initially and the interaction time is $t = 7.5(2\pi/\Delta)$. The narrowness of these peaks even at large values of the momentum splitting are the most important feature of this technique. The dashed line in figure 13 shows the predicted momentum scattering for thermal atomic beam with no common detuning, $\Delta = 80$ MHz, and $|\Omega| = 150$ MHz, and equal initial populations in all three atomic states. The vertical lines in figure 13 show preliminary experimental results for an effusive He beam using the $J = 1 \leftrightarrow J' = 1$ subsystem of the $2^3S_1$ to $2^3P_1$ transition in He, excited by a $\sigma_+$ polarized standing wave and a $\sigma_-$ polarized standing wave. In the experiment the initial populations were evenly distributed among the three ground states and the transverse momentum distribution was $\pm \hbar k$.

---

[19] T. Pfau, C.S. Adams, and J. Mlynek, *Europhys. Lett.* 21: 439 (1993).

[20] K. Johnson, J.D. Paul, A. Chu, M.S. Shahriar, K. Berggren, and M.G. Prentiss, Creating a Large Angle Coherent Atomic Beamsplitter without a Magnetic Field, 1994 IC Conference, forthcoming.

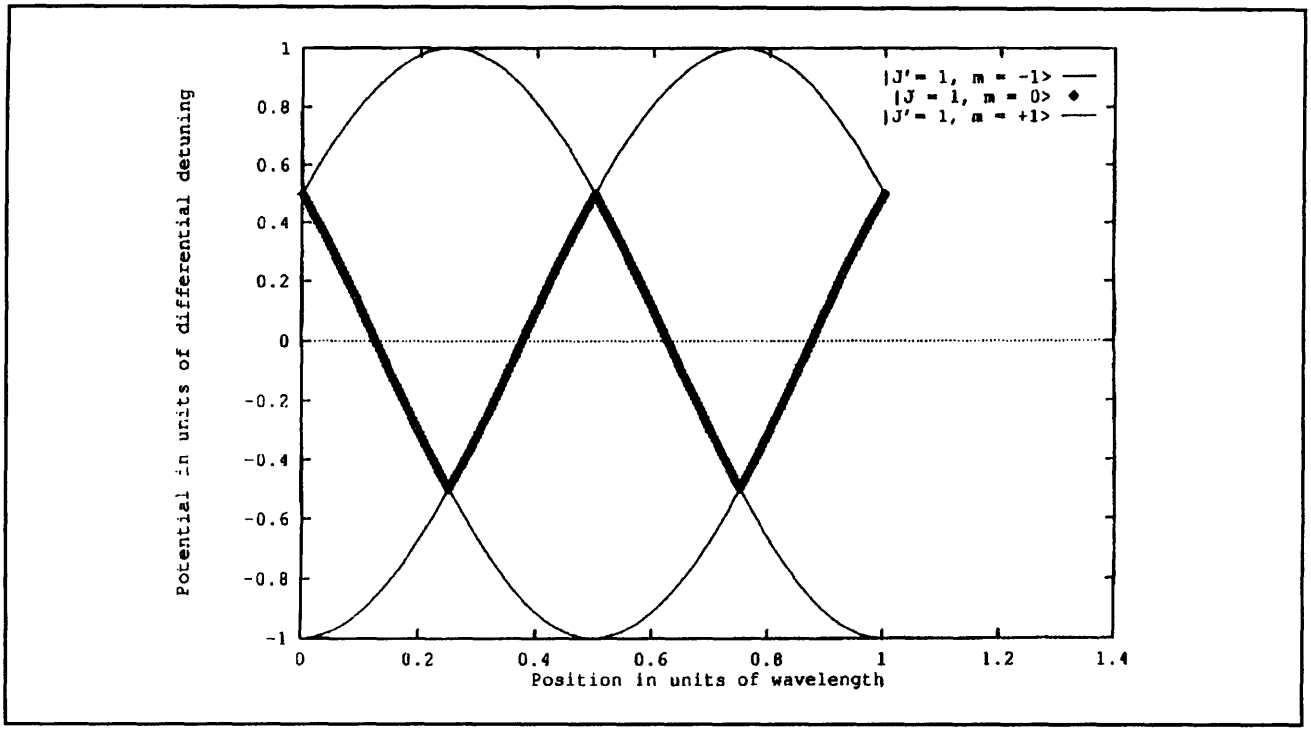


**Figure 11.** Eigenenergies as a function of position in the standing waves.

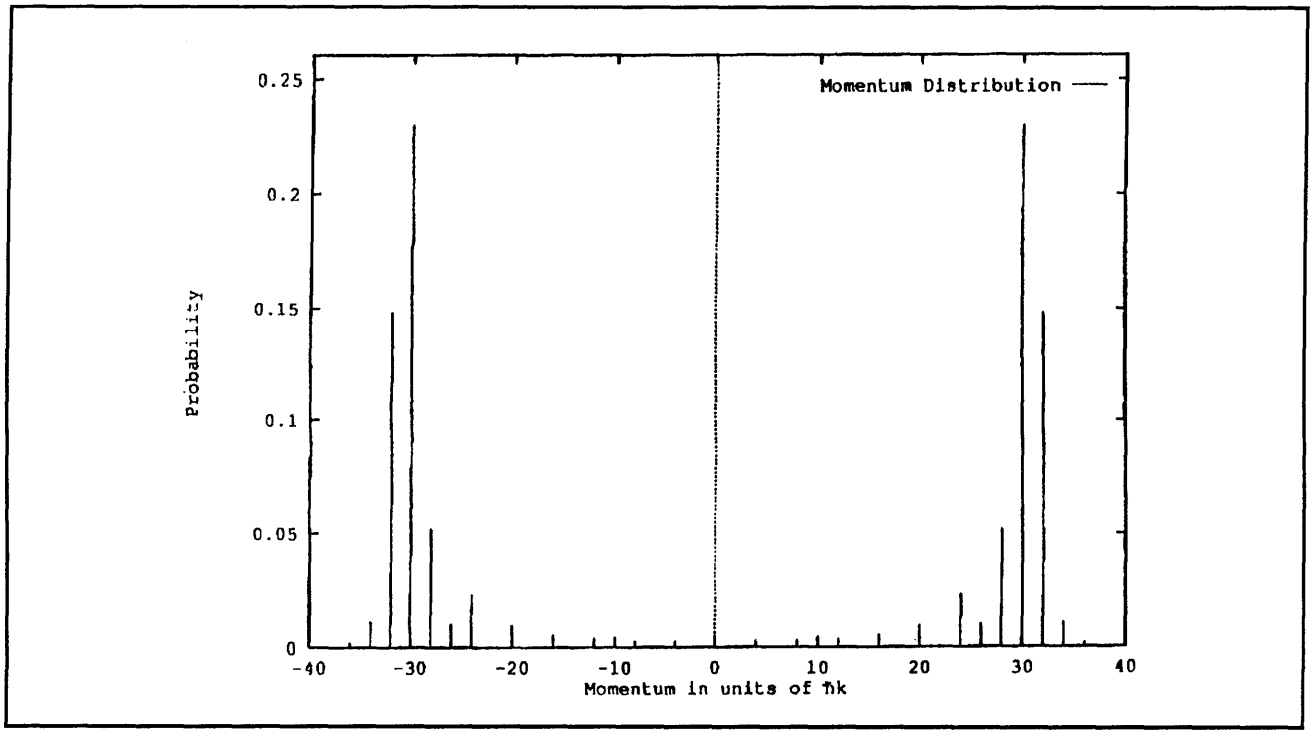


**Figure 12.** Theoretical momentum distribution for a monoenergetic atomic beam. The interaction time is $7.5(2\pi/\Delta)$ and each Rabi frequency is $\sqrt{2}\,\Delta$.

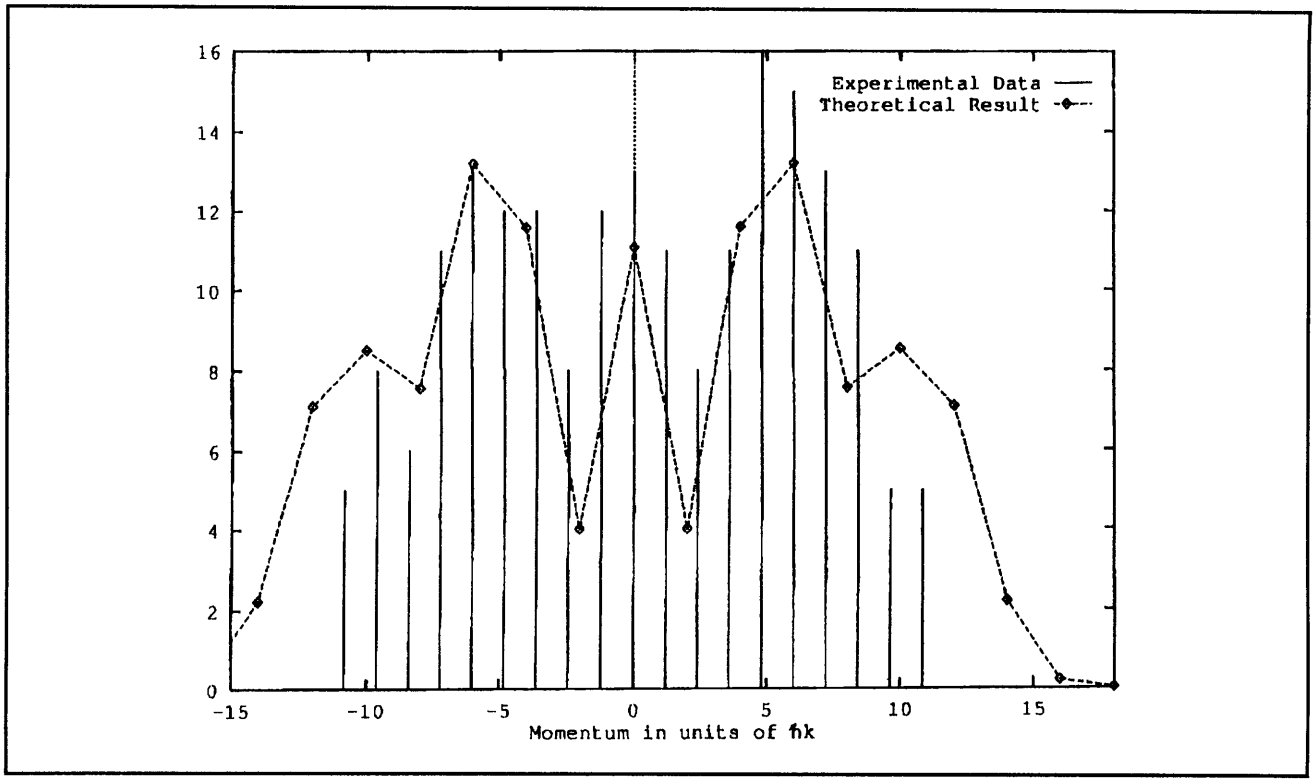


**Figure 13.** Preliminary experimental results for $\Delta = 80$ MHz, and each Rabi frequency of 150 MHz.

## 1.6 Stimulated Brillouin Scattering Ring Laser Gyroscope

### Sponsor

Charles S. Draper Laboratory
Contract DL-H-441690

Research is in progress on a new fiberoptic ring laser gyroscope based on two counter-propagating stimulated Brillouin scattering (SBS) lasers which are generated in the same fiberoptic ring resonator.[21] The use of SBS as the laser gain medium is crucial to the operation of this gyroscope because a conventional solid-state gain medium cannot support simultaneous bidirectional lasing due to gain competition between the counter-propagating lasers. The directionality of the SBS gain medium, however, prevents gain competition and thus allows stable, simultaneous bidirectional lasing.

In the presence of an inertial rotation normal to the plane of the ring laser's resonator, a difference frequency is automatically generated between the counterpropagating SBS lasers which is proportional to the applied rotation rate,[22] as predicted by the Sagnac effect. The operation of this solid-state gyroscope is very similar to that of the bulk-optic ring laser gyroscope (RLG) based on the He-Ne gain medium. It should be noted that gain competition in a gaseous medium is avoided by using two partially overlapping, Doppler broadened gain media.

In contrast with either the interferometer or passive resonator gyroscopes, both the SBS RLG and the He-Ne RLG do not require any external means to measure the nonreciprocal phase shift that is induced by rotation.

Figure 14 shows a simplified schematic diagram of an SBS ring laser gyroscope. Light from a 1 mW He-Ne laser at 1.15 $\mu$m is split into two pump beams, labeled P1 and P2, frequency shifted by acousto-optic modulators, and coupled into counter-propagating directions of the same ring resonator. For maximum effective pump power inside the

[21] S.P. Smith, F. Zarinetchi, and S. Ezekiel, "Fiberoptic Ring Laser Gyroscope," *Proceedings of the OFS '89,* Paris, France, 1989, post deadline paper.

[22] F. Zarinetchi, S.P. Smith, and S. Ezekiel, "Stimulated Brillouin Fiber-optic Laser Gyroscope," *Opt. Lett.* 16: 229-231 (1991).

resonator, the pump lasers are held at the centers of their respective cavity resonances using servos, not shown in the figure, and are matched to an eigen-polarization of the cavity resonance.

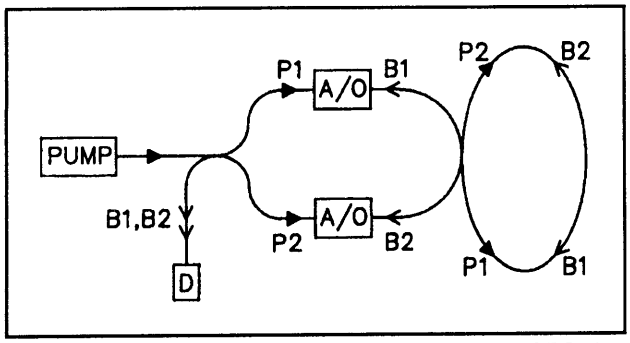


**Figure 14.** Simplified schematic diagram for a SBS ring laser gyroscope.

With the pump lasers above the SBS lasing threshold, 60 $\mu$W in this case, two SBS lasers, B1 and B2, are simultaneously generated in the resonator in directions opposite to that of their respective pump lasers. After leaving the cavity, the two SBS lasers are combined using a directional coupler and fall onto detector D.

Figure 15a shows the difference frequency between B1 and B2 when a sinusoidal rotation is applied to the gyroscope. As predicted by the Sagnac effect, the frequency difference varies linearly with the applied rotation rate, hence is 90 degrees out-of-phase with the applied rotation angle, as shown in figure 15b.

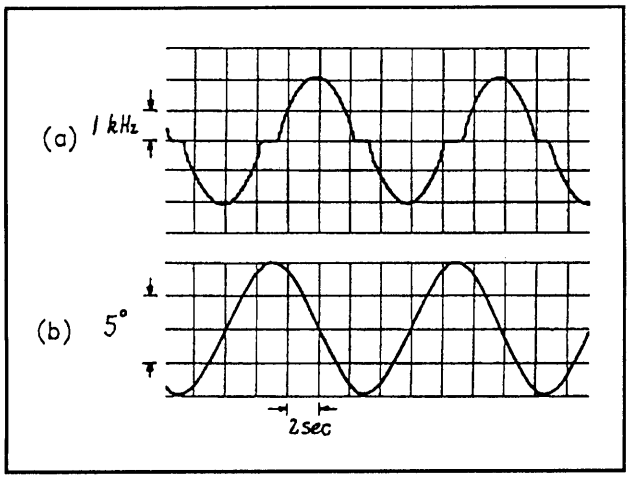


**Figure 15.** Simultaneous recording of (a) difference frequency between two counter-propagating SBS lasers and (b) the applied rotation angle.

However, it is important to note that for a range of low rotation rates in figure 15b the difference frequency between the SBS lasers is zero. This "lock-in" zone is caused by the frequency locking of the counter-propagating SBS lasers through backscattering within the cavity and has been extensively studied in the bulk-optic RLG where it is removed using mechanical dither.[23]

Mechanical rotation dither minimizes the amount of time that the gyroscope spends in the lock-in zone, thus reducing the errors due to lock-in. Because of its much smaller mass, mechanically dithering the fiber RLG would be much simpler than dithering the bulk-optic RLG.

Another method for removing lock-in is by generating the SBS lasers with a large frequency separation between them which would prevent the lasers from frequency locking. The tunability and directionality of the SBS gain medium allows the generation of the counter-propagating SBS lasers in different longitudinal modes of the resonator by either frequency shifting one of the pump lasers, or by using two separate pump lasers.

Figure 16a shows the difference frequency between two SBS lasers generated in different longitudinal modes of the same ring resonator, as a function of the applied rotation angle (figure 16b). In this case, the two lasers are separated by 9 longitudinal modes and, as seen in the figure, no lock-in is observed in the beat frequency.

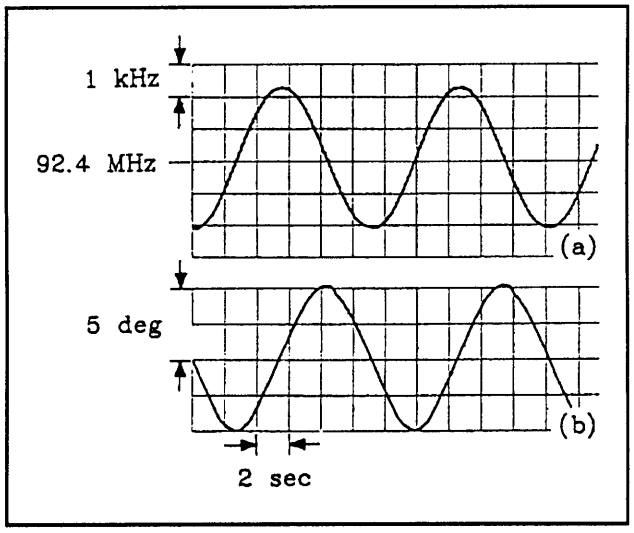


**Figure 16.** Lock-in free difference frequency (a) between two counter-propagating SBS lasers generated in different longitudinal modes of the resonator and (b) the applied rotation angle.

[23] F. Aronowitz, "The Laser Gyro," in *Laser Applications* (New York: Academic Press, 1971), vol. 1, pp. 133-200.

While this mode of operation eliminates errors due to lock-in, there are a number of additional sources of error unique to it. One important additional error source is due to dispersion pulling of the SBS laser frequencies resulting from intensity backscattering of the pump lasers.

Consider a single pump laser, P1, in the counter clockwise (19W) direction and the resulting SBS gain curve and SBS laser, B1, in the clockwise (CW) direction, as shown in figure 17. If there is any pump backscattering, a small amount of pump will also be present in the CW direction of the cavity, labeled P1′. Though this pump will be below the SBS lasing threshold, it will still generate a small SBS gain curve, labeled B1′. In a single direction SBS laser, this extra gain curve has no effect since it is in the opposite direction of the SBS laser.

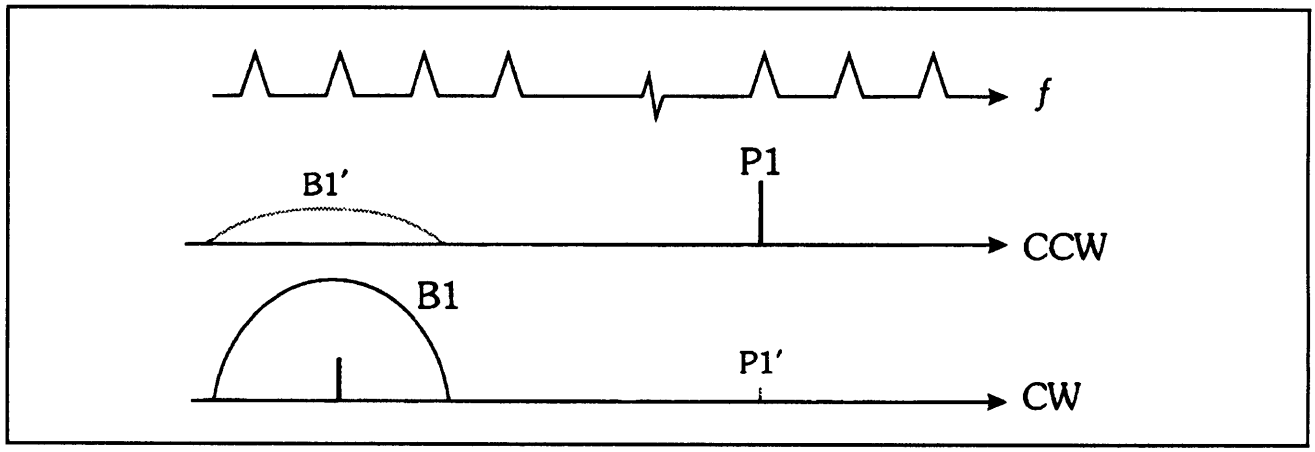


**Figure 17.** Generation of an extra SBS gain curve due to pump backscattering.

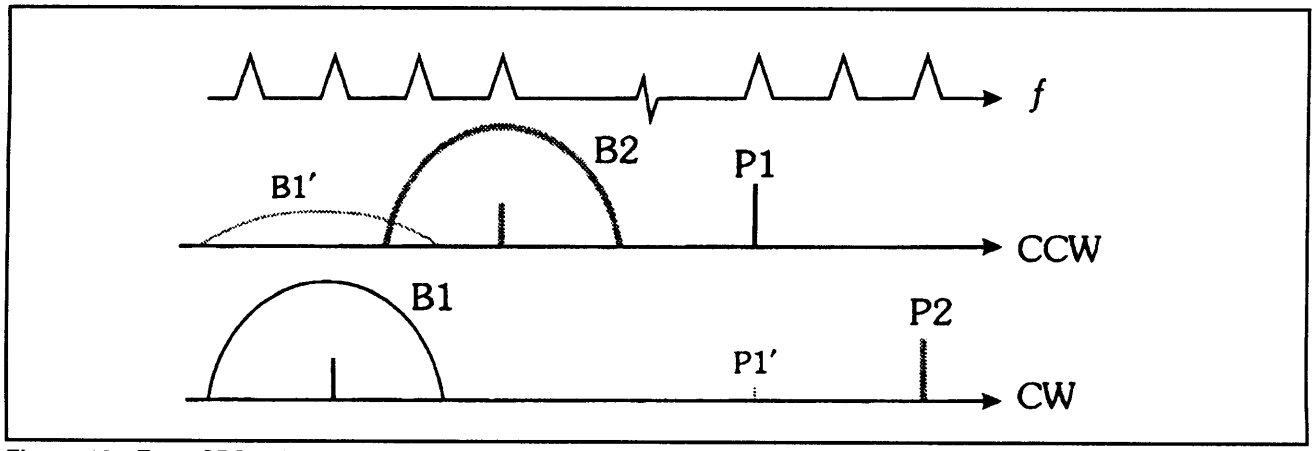


**Figure 18.** Extra SBS gain curve due to pump backscattering.

However, as shown in figure 18, if two counterpropagating SBS lasers, B1 and B2, are generated in the same cavity, this extra SBS gain curve, B1′, due to its dispersion, will pull the frequency of the B2 SBS laser. Thus, as the intensity of P1 changes, or as the backscattering at the pump frequency changes, the size of the dispersion pull will also change and cause a bias drift in the gyroscope. Further, since the intensity backscattering in the cavity is highly variable, the size of this dispersion pull is also highly variable.

The effect of this additional SBS again curve can be most easily demonstrated and measured by introducing a third pump laser into the cavity. In this way, the size and frequency separation of this third gain curve can be easily controlled. Figure 19 shows the effect of varying the intensity of the third pump laser on the beat frequency between the two SBS lasers. As seen in the figure, the frequency pull increases linearly with increasing pump power, as expected, and the maximum pulling was measured to be 680 Hz$\mu$W of input power. This is in good agreement with the predicted value of 700 Hz$\mu$W for this cavity.

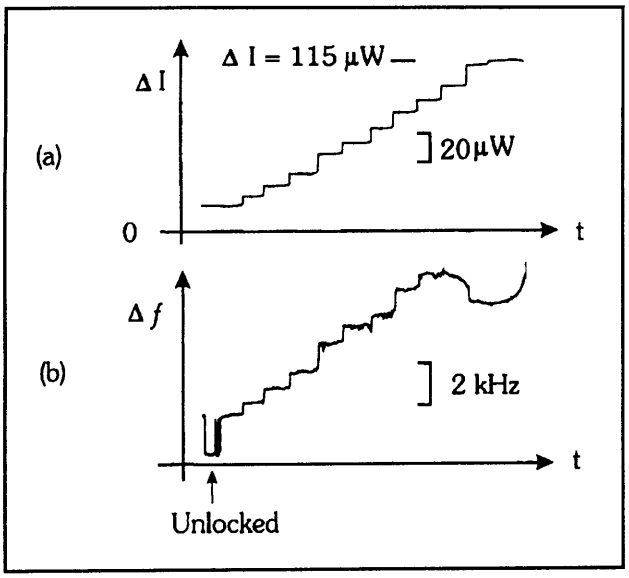


**Figure 19.** Dispersion pull versus third pump power. Note the saturation for higher pump powers is a result of the generation of a third SBS laser.

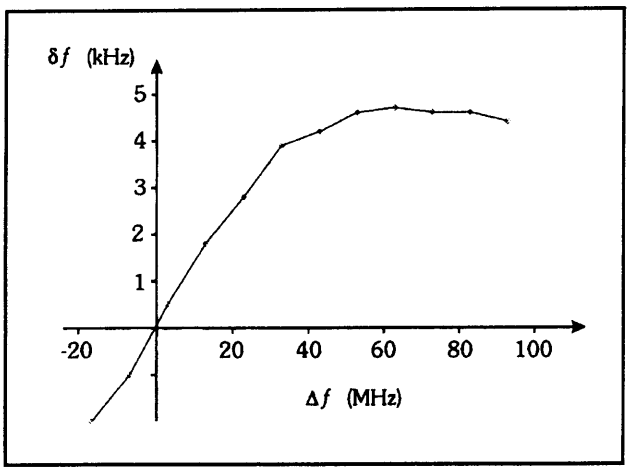


**Figure 20.** Dispersion pull as a function of third pump laser tuning.

In addition to measuring the dispersion pull versus pump power, the dispersion pull versus the frequency separation of the third pump laser can also be measured. Figure 20 shows the change in difference frequency between SBS lasers B1 and B2 as the frequency of the third pump laser is changed. As seen in the figure, the maximum dispersion pull occurs at approximately 70 MHz, indicating that the width of the SBS gain medium is approximately 140 MHz at 632 nm.

To reduce the errors due to dispersion pulls, SBS laser frequency spacings that are comparable to the half-width of the SBS gain curve should be avoided. Thus, either very large frequency spacings, or very small frequency spacings should be used.

Backscattering at the SBS laser frequencies also can lead to frequency pulls on the SBS lasers themselves. In this case, the frequency pull is the result of backscatter-induced changes in cavity loss at the SBS frequency which cause a change in the self dispersion pull due to the SBS laser's gain curve.

Normally, the internal losses of the cavity at the SBS frequency are considered to be constant. However, variations in backscattering can lead to significant variations in the cavity loss as a function of the cavity environment. This loss variation will cause a corresponding change in the SBS gain, since the gain always equals the loss while the SBS laser is lasing. Thus, if the cavity mode is not exactly at the center of the SBS gain curve, this variation in the SBS gain will cause a variation in the dispersion pull of the SBS gain curve. For example, for a cavity mode 70 MHz from the center of the SBS gain curve with a 100 $\mu$W threshold, a 1 percent variation in the cavity loss will result in a 680 Hz offset change.

This source of drift can be eliminated by thermally tuning the SBS gain curve so that the cavity resonance is at the center of the gain curve, since the dispersion is zero there.

Presently, though thermally and dispersively driven drifts appear to limit the performance of the separated frequency SBS fiber RLG, there are a number of other error sources which may become important as the performance improves. These errors include eigenpolarization mismatch between the SBS lasers which would reduce reciprocity between the SBS lasers, eigenpolarization mismatch between the pump and the SBS laser which could lead to polarization pulling, frequency pulls due to frequency dependent backscattering, and excess phase noise due to finite common mode suppression of cavity jitter.

In order to perform an independent test of the null stability, we are going to mechanically dither the SBS gyro. Mechanical dither, as in the case of the bulk-optic ring laser gyro, may very well prove to be the best alternative for eliminating lock-in.

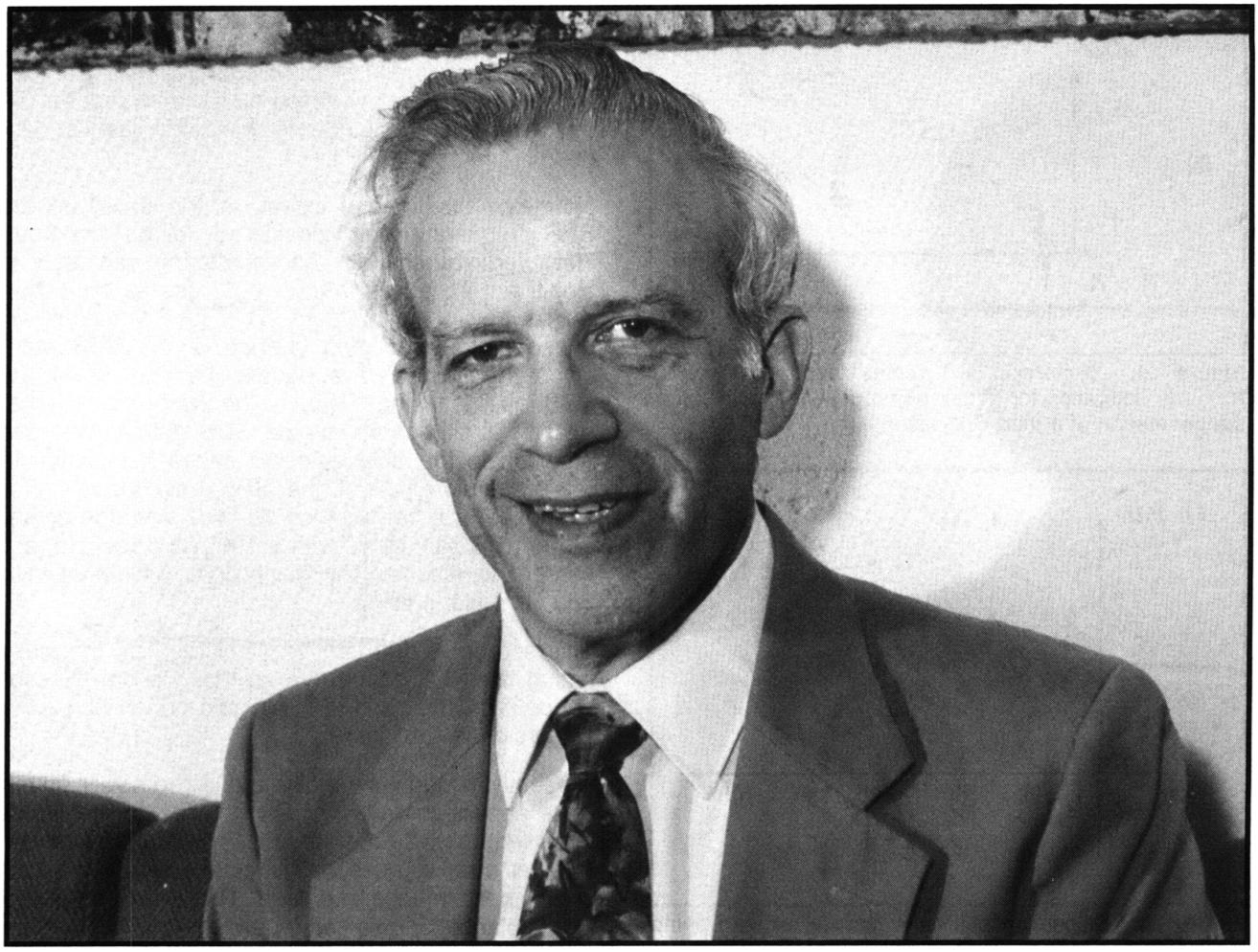

*Professor Daniel Kleppner, Associate Director of the Research Laboratory of Electronics*